Nonlinear effects and applications of AlN: A comprehensive physical formulation approach

A. F. Jaramillo-Alvarado, A. Torres Jacome, P. Rosales-Quintero, G. Diaz-Arango, and H. Vazquez-Leal

Electronics Department, Instituto Nacional de Astrofísica, Óptica y Electrónica,
e-mails: anfejaramillo@utp.edu.co; atorres@inaoep.mx; prosales@inaoep.mx; gerardo.diaz@itspozarica.edu.mx

Received 17 July 2023; accepted 13 September 2023

Piezoelectric materials have nonlinear effects that can be used in 5G and IoT technologies. However, since most nonlinear problems in this area do not have analytic solutions, FEM simulations are an essential design tool. In this study, we have developed a stress-charge formulation for non-linear piezoelectric materials compatible with commonly used simulation tools in industry and research. FEM simulation results for AlN with three nonlinear phenomena are presented: variation of effective electrical permittivity, shift of the effective elasticity constants and enhancement of electromechanical coupling factor. These simulations were conducted with the same material parameters, having great agreement with recent and important experimental results. The simulations allow us to deduce the values of the components of the high-order tensors for the first time as $q^r_{331} = q^r_{333} = -1600$ and $g_{333} = -80$ N/Vm. The maximum percent errors obtained for the simulations of the effective electrical permittivity and effective elasticity constants were 0.1% and 1.77%, respectively.

Keywords: Aluminum Nitride (AlN); nonlinear piezoelectric devices; nonlinear state equations; tunable devices; FEM simulation; tensor structure symmetry.

DOI: https://doi.org/10.31349/RevMexFis.70.011004

1. Introduction

One of the most important industries in the last three decades has been the semiconductor's industry which has a market capitalization of about $600B\$$ in 2022 [1]. Taking into account that Micro-electromechanical systems (MEMS) take up around 20% of the market [2], then the research in better materials, novel devices, and improvements in performance are fundamental to allowing the market growth.

AlN is a piezoelectric material that is used in a wide range of applications within the MEMS field, because of its great mechanical properties, enough chemical resistance to microfabrication processes, conventional deposition methods, and acceptable electromechanical coupling factor (k^2_{eff}) [3, 4]. The main linear applications where AlN is used as piezoelectric material are resonators [5, 6], tunable devices [7], several types of sensors [8], actuators [9], wearable devices [10], and generally where the layers at the microscale with piezoelectric effect are needed [11]. In all of those applications, the main characteristics offered by piezoelectric materials are low power consumption (around 10 μW), easy design techniques, CMOS compatibility, high operation frequencies, and high quality factor for frequency applications. Thus, this type of material is a suitable option to replace active devices in applications where these characteristics are needed.

Currently, in the context of the integrated circuits industry, the new technologies of the fifth generation of telecommunications (5G) and the Internet of Things (IoT) have demanding requirements that constrain devices to be designed with low power consumption, a peak data rate of 20 Gbit/s, low latency around 1 millisecond, and a high density of connections per unit area, as stated in Ref. [12]. To achieve these requirements, devices for 5G need to be capable of responding quickly, have wide bandwidth capabilities, consume less power, and be easy to design using modular techniques that allow for scalable implementations. Hardware requirements for IoT devices are similar to those for 5G technology [13]. But they also need to be compatible with energy harvesting and IC fabrication processes like CMOS, Fin FET, PD SOI, and FD SOI, where these demands can be accomplished by non-linear piezoelectric effects using AlN like as shown below.

In the field of sensors, nonlinear piezoelectric materials can be used to increase the sensibility of the sensors, as is shown in Ref. [14], where this effect is a result of two different phenomena: the variation of the effective electrical permittivity in the second order term and the shift of the resonance frequency generated by a high bias electric field. In the case of tunable resonators, a common method used is to bias the RF signal to stress the piezoelectric material, producing a shift of the resonance frequency [7, 15]. Within IoT applications, we have mainly two topics: wearable and energy harvester devices. For wearable devices, the AlN is a suitable option due to its biocompatibility, great performance in (101) oriented layers, and the capability to supply the self-powered devices [16]. In the energy harvesters field, the nonlinear effects can be used to enhance the value of V_{oc} by having a better performance. This effect can be obtained through two different ways, modifying the effective electrical permittivity or coupling piezoelectric tensor $d_{i\lambda}$ (strain-charge formulation) [17].

In general, the physical properties of piezoelectric materials can be modified by several nonlinear effects, which can be used to enhance the performance of devices. However, the

research on the nonlinear behavior of piezoelectric materials still has challenges for designers and engineers, particularly when it comes to modeling and predicting the material's behavior. Nonlinear effects can cause the material's response to be highly sensitive to small signal cases, making it difficult to accurately simulate the material's behavior using standard modeling techniques. Due to this reason, a first-principle and comprehensive physical formulation to model and predict the behavior in the nonlinear regime of piezoelectric materials is needed. In this work, we present a first principle formulation that met the requirements mentioned, as well as its implementation into a FEM simulator to compare the measurements of the state-of-the-art nonlinear devices that were carried out, resulting in errors that can be neglected in an industrial and research environment.

2. Nonlinear State Equations and Symmetries

Several thermodynamic potentials, constants, and physics conditions can be used to represent the physics behavior of a system. In this work, we use the approach of stress-charge formulation to develop the nonlinear state equations for piezoelectric materials. The starting point for this formulation is the total differential of the thermodynamic potential of the electric Gibbs function for the piezoelectric effect (the Einstein summation and Voigt conventions are assumed)

$$dG_2 = -D_k dE_k + T_\mu dS_\mu, \tag{1}$$

there, T_μ is the stress field, E_k is the electric field, S_μ is the deformation field, and D_k the electric displacement field, since piezoelectric materials belong to the perturbative nonlinear regime and are in a solid phase, the contributions of temperature and entropy are neglected.

In the theoretical development we assume that G_2 is continuous, has derivatives up to the third order, and being a total differential it meets the mixed derivatives equivalence theorem. Due to this, the total differentials of dependent variables can be written as

$$\begin{aligned} dT_\lambda &= C_{\lambda\mu} dS_\mu - e_{k\lambda} dE_k, \\ dD_i &= \epsilon_{ij} dE_j + e^T_{i\mu} dS_\mu, \end{aligned} \tag{2}$$

where $e^T_{k\lambda}$ are the piezoelectric coupling coefficients, $C_{\lambda\mu}$ is the elasticity constants and ϵ_{ij} is the electrical permittivity.

As can be proved, the G_2 allows to do Taylor expansion approximation around zero for Eqs. (2), then, using the mixed derivatives theorem, a conventional treatment on the thermodynamic potential G_2, and integration of the Taylor expansion, we can get the nonlinear state equation for piezoelectric materials

$$\begin{aligned} T_\lambda &= C_{\lambda\mu} S_\mu - e_{k\lambda} E_k \\ &\quad + \frac{t_{\lambda\mu\nu}}{2} S_\mu S_\nu + g_{\lambda\mu k} S_\mu E_k + \frac{q_{jk\lambda}}{2} E_j E_k, \\ D_i &= \epsilon_{ij} E_j + e^T_{i\mu} S_\mu \\ &\quad + \frac{r_{ijk}}{2} E_j E_k - q_{ij\lambda} E_j S_\lambda - \frac{g_{\lambda\nu i}}{2} S_\lambda S_\nu, \end{aligned} \tag{3}$$

where, the last terms of Eqs. (3) uses the Einstein convention in the form

$$\frac{r_{ijk}}{2} E_j E_k = \sum_{n=1}^{3} \frac{r_{inn}}{2} E_n E_n.$$

Taking into account the algebraic conditions of Einsten and Voigt conventions, algebraic coefficient terms are not needed between representations (canonical and Voigt), since

$$\begin{aligned} t_{\lambda\mu\nu} &= t_{ijklmn}, \quad g_{\lambda\mu m} = g_{ijklm}, \\ q_{jk\lambda} &= q_{jklm} \quad \forall\, \lambda, \mu, \nu \in [1, 6]. \end{aligned}$$

Finally, the remaining tensors to be defined are

$$\begin{aligned} \frac{\partial^2 T_\lambda}{\partial E_j \partial E_k} &= -\frac{\partial^2 D_k}{\partial S_\lambda \partial E_j} = -\frac{\partial^2 D_k}{\partial E_j \partial S_\lambda} = q_{kj\lambda} - \frac{\partial^2 D_k}{\partial S_\lambda \partial S_\mu} \\ &= \frac{\partial^2 T_\lambda}{\partial E_k \partial S_\mu} = \frac{\partial^2 T_\lambda}{\partial S_\mu \partial E_k} = g_{\lambda\mu k} \frac{\partial^2 D_i}{\partial E_j \partial E_k} \\ &= r_{ijk}, \frac{\partial^2 T_\lambda}{\partial S_\mu \partial S_\nu} = t_{\lambda\mu\nu}, \end{aligned} \tag{4}$$

where their interpretation are the following. The term $g_{\lambda\mu k} S_\mu E_k$ is the correction term for the elastic constants when a high electric field is present. This phenomenon results in changes to the elastic behavior through the elasto-electric effect. $q_{ij\lambda} E_j S_\lambda$ represents the contribution to the electric permittivity due to the strains S_λ associated with the anisotropy of piezoelectric behavior with respect to E_j. The $t_{\lambda\mu\nu}$ tensor adjust the nonlinear behavior of the stress field in response to the relationship between the strains S_μ and S_ν within the strong deformations range, even though the measurements are taken in the linear deformation range. Similarly, the r_{ijk} tensor changes the electric displacement vector due to the dielectric quadratic behavior of the material, this tensor is associated with the anisotropy relationship between E_j and E_k with respect to the displacement vector.

Now, is needed to introduce some definitions that allows us simulate nonlinear piezoelectric devices in FEM software, we define

$$C^{eff}_{\lambda\mu} = C_{\lambda\mu} + g_{\lambda\mu k} E_k, \tag{5}$$

$$\begin{aligned} \varepsilon^{eff}_{ij} &= \varepsilon_0 \varepsilon^{r-eff}_{ij} = \varepsilon_0 \left(\varepsilon^r_{ij} - \frac{q_{ij\lambda} S_\lambda}{\varepsilon_0} \right) \\ &= \varepsilon_0 \left(\varepsilon^r_{ij} - q^r_{ij\lambda} S_\lambda \right), \end{aligned} \tag{6}$$

where $C_{\lambda\mu}^{eff}$ is the effective elasticity constants, ϵ_0 the vacuum permittivity, ϵ_{ij}^{r} corresponds with the relative permittivity, ε_{ij}^{r-eff} is the effective relative permittivity and $q_{ij\lambda}^{r}$ is the $q_{ij\lambda}$ tensor divided by the vacuum permittivity. To state the above equations, we consider

$$\epsilon_{ij}^{eff} = \epsilon_{ij} - q_{ij\lambda} S_{\lambda}.$$

To simulate nonlinear piezoelectric devices with FEM software, it is mandatory to have the symmetry structure of the four high-order tensors of Eqs. (3). This process starts with the transformation laws for tensors and their symmetry generators a_{ij} of each crystalline structure. Here we show the deduction of transformation law for $e_{k\lambda}$, the other transformation laws follow an analogous process. We start with the transformation laws of stress and electric fields

$$T_{\lambda}^{'} = M_{\lambda\beta} T_{\beta} \ , \quad E_{i}^{'} = a_{ij} E_{j}, \tag{7}$$

where $T_{\lambda}^{'}$ and $E_{\mu}^{'}$ represent the stress and electric fields after transformation (*e.g.* rotation), and $M_{\lambda\beta}$ is the transformation matrix which is a function of the specific symmetry generator a_{ij} of the crystal; the form of $M_{\lambda\beta}$ and a_{ij} can be found in Ref. [18]. Now, we can use the respective algebraic term from state equation, so

$$T_{\beta} = -e_{k\beta} E_{k},$$

then, after replacing Eq. (7), is obtained

$$T_{\lambda}^{'} = -M_{\lambda\beta} \ e_{k\beta} \ a_{ik}^{-1} \ E_{i}^{'},$$

where the transformation law for $e_{k\lambda}$ tensor is deduced as

$$e_{\lambda i}^{'} = M_{\lambda\beta} \ e_{k\beta} \ a_{ik}^{-1}. \tag{8}$$

By an analogous deduction, we obtain the transformation laws for high-order tensors

$$\begin{aligned} g_{\lambda\mu k}^{'} &= M_{\lambda\beta} N_{\nu\mu}^{-1} a_{mk}^{-1} \ g_{\beta\nu m}, \\ q_{jk\lambda}^{'} &= M_{\lambda\beta} a_{lj}^{-1} a_{mk}^{-1} \ q_{lm\beta}, \\ r_{ijk}^{'} &= a_{il} a_{mj}^{-1} a_{nk}^{-1} \ r_{lmn}, \\ t_{\lambda\mu\nu}^{'} &= M_{\lambda\alpha} N_{\beta\mu}^{-1} N_{\gamma\nu}^{-1} \ t_{\alpha\beta\gamma}. \end{aligned} \tag{9}$$

The calculation of the structure of the tensors can be achieved through the use of transformation laws (Eqs. (9)) and generators of specific crystal or point group (a_{ij}). We also use two additional constraints: the equivalence between the last two sub-indexes $t_{\lambda\mu\nu} = t_{\lambda\nu\mu}$ and knowing that the generators meet $a_{ij}^{-1} = a_{ij}^{T}$ since they all belong to the SO(3) group. Using these conditions, we obtain an indeterminate algebraic system that, after solving, we obtain the symmetry structure of the crystal system for the specific generators used.

After getting all the symmetry structures of crystal systems, we determine that all crystal classes have $q_{ij\lambda}$ and $t_{\lambda\mu\nu}$ tensors different from zero, while $g_{\lambda\mu k}$ and r_{ijk} tensors are zero unless the material demonstrates the linear piezoelectric effect. The only exception to these rules is the 432 point group where r_{ijk} remains equal to zero but $g_{\lambda\mu k}$ is non-zero. The symmetry structure of the tensors is vast; for this reason, Table I only shows the non-zero tensor components of AlN.

TABLE I. Nonzero components of $g_{\lambda\mu k}$, $q_{ij\lambda}$ and r_{ijk} tensors for the stress-charge formulation of some commonly used piezoelectric materials in industry.

Material	Crystal Class	$g_{\lambda\mu k}$	$q_{ij\lambda}$	r_{ijk}
AlN	6 mm	151,251,351, 461,142,242, 342,562,113, 123,133,223, 233,333,443, 553,663	111,221,331, 112,222,332, 113,223,333, 234,135,126	131,232,113, 223,333

3. Nonlinear effects and applications of AlN

The nonlinear effects of AlN appear at strong deformations or high electric fields; this results in a hysteresis behavior (as a soft ferroelectric effect), variation of the effective relative permittivity, deviation of elasticity constants, and changes in the electromechanical coupling factor k_{eff}^{2}. Table II shows the estimated value of high-order tensors and the regimen for electric field excitation that raises the nonlinear effects on AlN, these estimations were conducted through an exhaustive review of literature on the nonlinear effects of AlN.

The hysteresis behavior of AlN is due to two main factors: changes in domain walls and the re-alignment of unit cell dipoles, both induced by external electric fields [19–21]; this effect is used mainly in memories [22]. Physically, the contribution of these factors to the stress and displacement fields is quantified through $q_{kj\lambda}$ tensor since the change in domain walls leads to a spontaneous strain that contributes to the stress field, as shown in the first equation of Eqs. (3). While the alignment of unit cell dipoles results in a spontaneous polarization field that contributes to the displacement vector field taken into account in the second equation of Eqs. (3).

The change in electrical permittivity due to the nonlinear effect in piezoelectric materials is produced by the change in charge density in the unit cell of the crystal, this phenomenon is provoked by strong deformations [14], and can be used in devices like tunable capacitors or resonators. This effect is taken into account by the term $q_{ij\lambda} E_{j} S_{\lambda}$ from Eqs. (3).

The most commonly used nonlinear effect in piezoelectric materials is the change in the elasticity constants, which is induced by the shift of the inter-atomic forces due to strong deformations resulting in the variation of the stiffness of the material. This effect can be found in the literature such as elasto-electric effect or nonlinear electro-estriction [23].

TABLE II. Estimated order of magnitude of high-order tensors and range of electric excitement for the appearing of nonlinear effects in AlN.

Material Parameter	Symbol	Order	Nonlinear effects raises at	Units
Strain correction term for strong deformations	$t_{\lambda\mu\nu}$	$10^{10} - 10^{12}$	N/A	N/m^2
Electrical correction term for quadratic behavior of displacement vector	r_{ijk}	$10^{-20} - 10^{-22}$	10^9 V/m	C/V^2
Electrical correction term of elasticity constants and piezoelectric coefficients	$g_{\lambda\mu k}$	$10^{1} - 10^{3}$	10^6 V/m	C/m^2
Strain correction term of electrical permittivity and piezoelectric coefficients	$q_{ij\lambda}$	$10^{-10} - 10^{-8}$	10^7 V/m	N/Vm

Usually, this effect is used by tunable resonators and high precision sensors [7] to shift the resonance or operation frequency through a DC voltage. The formulation presented models this effect through the term $g_{\lambda\mu k}S_\mu E_k$ in Eqs. (3).

A measurement of the capability of transduction for piezoelectric materials is the electromechanical coupling factor k^2_{eff}, which depends on the main oscillation mode of the system, which is defined as

$$k^2_{eff} = \frac{(e^{eff}_{x5})^2}{C^{eff}_{44}\epsilon^{eff}_{xx}} , \tag{10}$$

for a device with a Z-shear oscillation mode and a wave in the X-propagation axis. Eq. (10) shows that the effective elasticity constants have the most significant impact on k^2_{eff} since they have a greater order variation. Therefore, when the resonance frequency shifts, the electromechanical coupling factor increases while the effective elasticity constants decrease. Consequently, for applications such as energy harvesters, microphones, etc., where power transduction is a key factor, a negative bias DC electric field enhances the performance of the device [24].

4. Simulations and results

To implement the theoretical formulation presented in this paper, we have chosen three independent experimental studies to compare their measurements with respect to the four results obtained from FEM simulations for effective electrical permittivity [25], effective elasticity constant, electromechanical coupling factor [7] and impedance/admittance behavior [26]. All simulations use the same material parameters and AlN as a piezoelectric layer. Also, the components of tensors that the simulation must take into account are g_{333}, q_{331} and q_{333} since the main oscillation mode of devices uses those components only. The values obtained by adjusting the simulation results with the corresponding experimental data for the tensor components were

$$q^r_{331} = q^r_{333} = -1600 \text{ and } g_{333} = -80 \text{ N/Vm}. \tag{11}$$

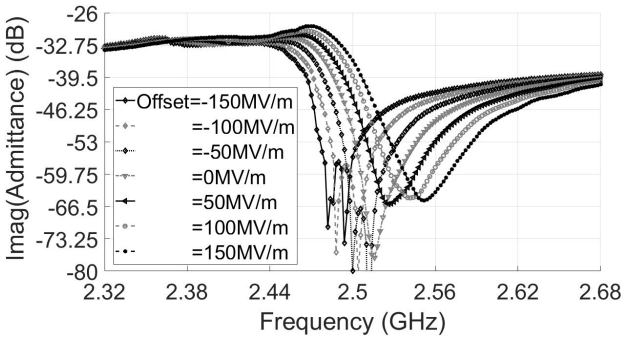

FIGURE 1. Resonance frequency obtained from simulation for device fabricated in Ref. [7], the shift of the resonance frequency is due to the electro-elastic effect.

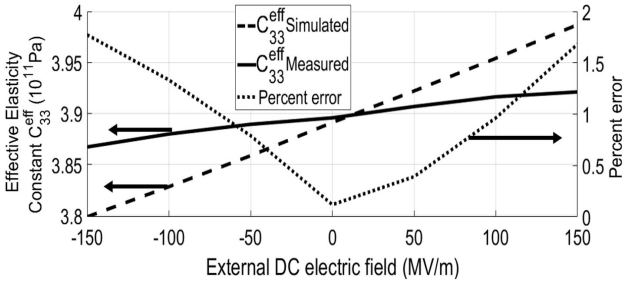

FIGURE 2. Effective elasticity constant C^{eff}_{33} of the device measured [7] and simulated (left axis), and the percent error (right axis) for the simulation that includes the nonlinear effects of $g_{\lambda\mu k}$ and $q_{ij\lambda}$ tensors.

In Fig. 1 is shown the shift of the resonance frequency obtained from simulations that replicate the experimental behavior is due to the elasto-electric effect of the device fabricated in Ref. [7]. The corresponding effective elasticity constant C^{eff}_{33} measured and simulated is presented in Fig. 2, where the simulation results were obtained through the formulation presented in this work, the maximum and average percent errors obtained were 1.77% and 1.0% respectively. The nonlinear effect of the shift of the elasticity constant that appears in this measurement was modeled by the Eq. (5) and the g_{333} tensor component.

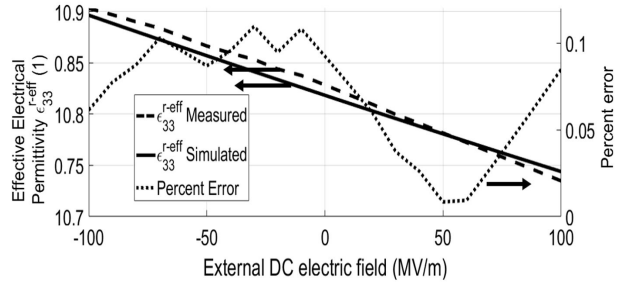

FIGURE 3. Effective relative electrical permittivity ϵ_{33}^{r-eff} of the device fabricated [25] and simulated (left axis), and the percent error (right axis) for the simulation that includes the nonlinear effects of $g_{\lambda\mu k}$ and $q_{ij\lambda}$ tensors.

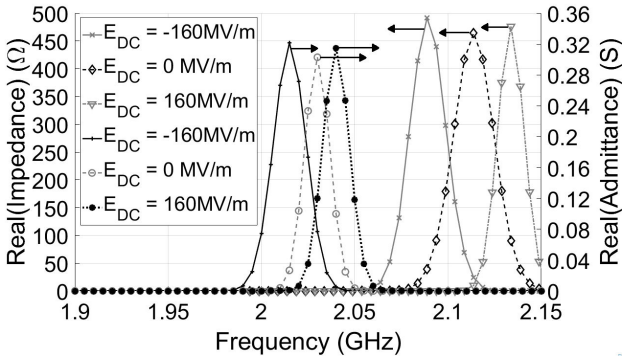

FIGURE 4. Real part of admittance and impedance obtained from simulations that includes the physics formulation presented for device fabricated and measured in Ref. [26]. The correction terms of the tensors $g_{\lambda\mu k}$ and $q_{ij\lambda}$ change the electrical-behavior of the device under high electric fields.

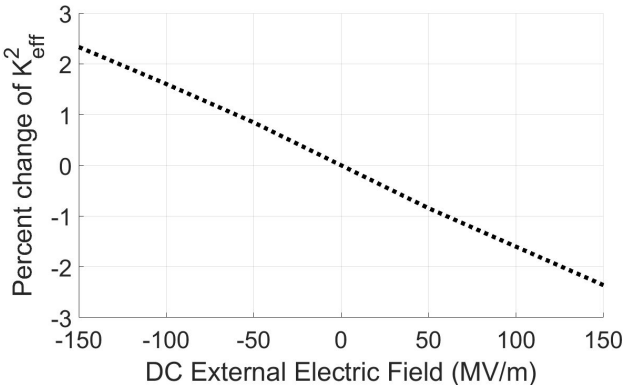

FIGURE 5. Electromechanical coupling factor k_{eff}^2 obtained from simulations that includes the physics formulation presented, replicating the nonlinear effects observed in the experimental measurements made in Refs. [7, 25, 26].

In Fig. 3 the effective relative permittivity obtained from measurements and simulations is presented, and the nonlinear effect that modifies the electrical permittivity was introduced to simulation through the programming of Eq. (6). Also, the maximum and average percent errors obtained for this case were 0.1% and 0.069% respectively. This effect is due to the inclusion of q_{331}^r in the simulation calculus with the physics formulation presented in this work.

The admittance and impedance behavior for the device fabricated in Ref. [26] were replicated with the same simulation parameters used in the previous results. In Fig. 4 are shown in the same structure of measurements the real part of impedance and admittance, where the maximum percent error obtained was 1.2% and 0.8% for the measurement of anti-resonance and resonance frequencies respectively.

The behavior of the electromechanical coupling factor k_{eff}^2 can be observed in Fig. 5. The measurement of this parameter is not shown in the references replicated, but we can extract it from simulations since all of them have the same material parameters and main oscillation mode, so the value of k_{eff}^2 is the same.

Finally, the simulation results expose that the stress-charge nonlinear state equations implemented in FEM simulations align well with the nonlinear effects of change of the elasticity constants and variation of electrical permittivity phenomena presented in AlN, as well as with the electromechanical coupling factor, which depends on these physical parameters.

5. Conclusion

This work shows the state equations in the stress-charge formulation to model the non-linear piezoelectric behavior based on thermodynamics and first principles. By applying the transformation laws, we determined the non-zero values of high-order tensors for the crystal symmetry of AlN. Also, FEM simulations that include the formulation presented were conducted to replicate the nonlinear effects exposed in Refs. [7, 25, 26], specifically the change of electrical permittivity, variation of elasticity constants, and the behavior of electromechanical coupling factor using the tensor components needed for fabricated AlN devices, where the components used are $g_{333} = -80$ N/Vm and $q^r331 = q^r333 = -1600$. Our simulations predicted the nonlinear effects with great accuracy, presenting maximum percent errors of 1.77% and 0.1% for the effective elasticity constants and effective relative electrical permittivity, respectively. These results demonstrate the effectiveness of our approach to predicting nonlinear effects in piezoelectric devices. For this reason, a design methodology based on FEM simulations using Eqs. (3), (5) and (6) is useful for industrial and research applications in emerging technologies where low power consumption, high operating frequencies, and wide bandwidth are needed features.

Acknowledgment

The authors acknowledge Instituto Nacional de Astrofísica, Óptica y Electrónica (INAOE) by its support under Colaboración scholarship.

1. Semiconductor-Industry-Association, State of The U.S. Semiconductor Industry (2022).
2. Future-Market-Insights, Future Market Insights, Microelectromechanical System (MEMS) Market Outlook (2022-2029) (2022).
3. C. Fei *et al.*, AlN piezoelectric thin films for energy harvesting and acoustic devices, *Nano Energy* **51** (2018) 146, https://doi.org/10.1016/j.nanoen.2018.06.062.
4. P. Muralt, Recent Progress in Materials Issues for Piezoelectric MEMS, *Journal of the American Ceramic Society* **91** (2008) 1385, https://doi.org/10.1111/j.1551-2916.2008.02421.x.
5. M. Rinaldi *et al.*, Super-high-frequency two-port AlN contour-mode resonators for RF applications, IEEE Transactions on Ultrasonics, *Ferroelectrics, and Frequency Control* **57** (2010) 38, https://doi.org/10.1109/TUFFC.2010.1376.
6. G.-H. Feng *et al.*, Investigation of Mo Doping Effects on the Properties of AlN-Based Piezoelectric Films Using a Sputtering Technique, *ECS Journal of Solid State Science and Technology* **11** (2022) 123005, https://doi.org/10.1149/2162-8777/aca796.
7. C. Chen *et al.*, Electric Field Stiffening Effect in c-Oriented Aluminum Nitride Piezoelectric Thin Films, *ACS Applied Materials & Interfaces* **10** (2018) 1819, https://doi.org/10.1021/acsami.7b14759.
8. P. Shanmugam *et al.*, Broad bandwidth air-coupled micromachined ultrasonic transducers for gas sensing, *Ultrasonics* **114** (2021) 106410, https://doi.org/10.1016/j.ultras.2021.106410.
9. K. Ruotsalainen *et al.*, Resonating AlN-thin film MEMS mirror with digital control, *Journal of Optical Microsystems* **2** (2022) 011006, https://doi.org/10.1117/1.JOM.2.1.011006.
10. Y. Wu *et al.*, Piezoelectric materials for flexible and wearable electronics: A review, *Materials Design* **211** (2021) 110164, https://doi.org/10.1016/j.matdes.2021.110164.
11. M.-I. Choe and K.-H. Kim, Second-Order Nonlinear Optical Responses of AlN Two-Dimensional Monolayer: A Real-Time First-Principles Study, *Chem. Phys. Chem.* **23** (2022) e202100901, https://doi.org/10.1002/cphc.202100901.
12. ITU-R, IMT Vision - Framework and overall objectives of the future development of IMT for 2020 and beyond, e-print https://www.itu.int/rec/R-REC-M.2083-0-201509-I.
13. S. Alam *et al.*, Internet of Things (IoT) Enabling Technologies, Requirements, and Security Challenges, In M. L. Kolhe *et al.*, eds., *Advances in Data and Information Sciences* (Springer Singapore, Singapore, 2020) pp. 119.
14. Z. Luo *et al.*, Nonlinearity of Piezoelectric Micromachined Ultrasonic Transducer Using AlN Thin Film, *IEEE Open Journal of Ultrasonics, Ferroelectrics, and Frequency Control* **2** (2022) 96, https://doi.org/10.1109/OJUFFC.2022.3182926.
15. G. Piazza *et al.*, High-Efficiency Piezoelectric-Transducer-Tuned Feedback Microstrip Ring-Resonator Oscillators Operating at High Resonant Frequencies, *IEEE Transactions On MicrowaveTheory And Techniques* **51** (2003) 1141.
16. M. Sawane and M. Prasad, MEMS piezoelectric sensor for self-powered devices: A review, *Materials Science in Semiconductor Processing* **158** (2023) 107324, https://doi.org/10.1016/j.mssp.2023.107324.
17. S. S. Chauhan, M. M. Joglekar, and S. K. Manhas, High Power Density CMOS Compatible Micro-Machined MEMs Energy Harvester, *IEEE Sensors Journal* **19** (2019) 9122, https://doi.org/10.1109/JSEN.2019.2923972.
18. B. A. Auld, *Acoustic Fields And Waves In Solids*, **1** (1973) 73.
19. Modeling Rate-dependent Hysteresis in Piezoelectric Actuators, IEEE International Conference on Intelligent Robots and Systems.
20. G. Bertotti and I. D. Mayergoyz, *The Science of Hysteresis*, **3** (2005) 337.
21. R. C. SMITH, A Domain Wall Model for Hysteresis in Piezoelectric Materials, *Journal Of Intelligent Material Systems And Structures* **11** (2000)
22. L. Xu *et al.*, Organic Enantiomeric Ferroelectrics with High Piezoelectric Performance: Imidazolium l- and d- Camphorsulfonate, *Chemistry of Materials* **33** (2021) 5769, https://doi.org/10.1021/acs.chemmater.1c01663.
23. The Effect Of Static Electric Fields On The Elastic Constants of alpha-Quartz, SPIE Smart Structures + Nondestructive Evaluation.
24. H. Liu *et al.*, A comprehensive review on piezoelectric energy harvesting technology: Materials, mechanisms, and applications, *Applied Physics Reviews* **5** (2018) 041306, https://doi.org/10.1063/1.5074184.
25. N. B. Hassine *et al.*, Linear variation of aluminum nitride capacitance versus voltage induced by a piezoelectricelectrostrictive coupling, *Journal of Applied Physics* **104** (2008)
26. E. Defaÿ *et al.*, Tunability of Alluminum Nitride Acoustic Resonators: A Phenomenological Approach, *IEEE Transactions on Ultrasonics, Ferroelectrics, and Frequency Control* **58** (2011) 2516, https://doi.org/10.1109/TUFFC.2011.2114.